Performance of UWB Receivers with Partial CSI Using a Simple Body Area Network Channel Model

Thomas Zasowski, *Member, IEEE*, and Armin Wittneben, *Member, IEEE*

***Abstract*— Ultra wideband (UWB) communication is a very promising candidate for the use in wireless body area networks (BAN). The high UWB peak data rate allows for medium average data rates in combination with a very low duty cycle, which is the key for a very low power consumption. Devices in a wireless BAN require low complexity. Hence, mainly non-coherent receivers such as energy detector and transmitted-reference receiver are suited. In this paper, the symbol-wise maximum-likelihood (ML) detectors for pulse position modulation (PPM) and transmitted-reference pulse amplitude modulation (TR PAM) are derived assuming partial channel state information (CSI) at the receiver. Additionally, also the ML detectors for a combination of PPM and TR PAM are presented. The performance of the derived receiver structures is evaluated using a novel BAN channel model not distinguishing line-of-sight and non line-of-sight situations. This simple channel model is based on 1100 channel measurements in the frequency range between 2 and 8 GHz, which were measured in an anechoic chamber. Using the BAN channel model, performance of the derived receiver structures is evaluated showing that the knowledge of the average power delay profile (APDP) at the receiver improves performance substantially. Requiring only slightly more complexity such receivers are a well suited alternative to non-coherent receivers for the use in a BAN.**

***Index Terms*— Body Area Network, Ultra Wideband, Channel Model, Non-coherent Receiver Structures**

I. Introduction

ONE OF THE most promising technologies for the use in wireless body area networks is ultra wideband (UWB) communications. Due to the relatively small delay spread and the moderate path loss in a body area network (BAN), very high peak data rates can be achieved with this technology. Medium data rate systems with ultra low power consumption can be realized using a very low duty cycle operation with high peak data rates. Recently, an energy detection based UWB transceiver structure for wireless sensor networks and BAN was presented [3] with an estimated power consumption of less than 1 mW. There, the average data rate of 500 kbps is realized by a transmission with 1 % duty cycle and a peak data rate of 50 Mbps.

Coherent receivers as e.g. rake receivers are much too complex for the use in a BAN. As shown in [4] the number of required rake fingers is only small for very short distances between transmitter and receiver. Moreover, coherent receivers require a channel estimation, which needs too high complexity for many BAN applications. Therefore, non- or semi-coherent receiver structures are most promising for the use in a BAN. Two modulation schemes that are often used in combination with non-coherent receiver structures are pulse position modulation (PPM) and transmitted reference pulse amplitude modulation (TR PAM). In PPM systems, data is transmitted by using different pulse positions for the different bit values. In transmitted reference (TR) systems a doublet consisting of two pulses is transmitted. One pulse is the reference pulse, which serves as a noisy template for correlation in the receiver, while the second one is the data pulse. Hence, in TR PAM systems the data is modulated in the amplitude of the data pulse. Often, these modulation schemes are considered together with an energy detector in a case of PPM [5] or a correlator in case of TR PAM [6]. A combination of PPM and TR PAM was presented in [7]. This modulation scheme, where the data is not only contained in the amplitude of the data pulse but also in its position, is referred to as transmitted reference pulse interval amplitude modulation (TR PIAM) in the remainder. A suboptimum receiver structure for TR PIAM was introduced in [7] requiring two correlation receivers with different delays. Although the complexity of the TR PIAM receiver is higher compared to the one of a TR PAM correlation receiver it is still reasonable and performance is much better. The receiver structures with lowest complexity are the energy detector and the TR PAM correlation receiver, which both do not require a channel estimation. However, there may also exist nodes in a BAN that allow for slightly higher complexity such as a master node. Therefore, we investigate the impact of partial channel state information (CSI) at the receiver on the detection performance. Assuming the knowledge of the average power delay profile (APDP) at the receiver, the symbol-wise maximum-likelihood (ML) detectors for PPM, TR PAM, and TR PIAM are derived. For comparison reasons also the receiver structures for full CSI and without CSI are presented.

The performance of the different receiver structures shall be evaluated on basis of a simple channel model for UWB BAN. The IEEE 802.15.4a BAN channel modeling group specified a channel model for UWB BAN [8]. However, this model is based on finite difference time domain (FDTD) simulations with 2 GHz bandwidth and cannot be adapted to larger bandwidths. There also exists a channel model for UWB BAN in the frequency range between 3 and 6 GHz where the transmitter has been placed on the front side of the torso and the receiver on various positions around the torso [9]. This

Manuscript received January 15, 2008; revised September 28, 2008. This paper is presented in part at the International Conference on Ultra Wideband (ICUWB) 2006, Waltham, MA, USA, September 2006 [1] and at the IEEE International Symposium on Personal, Indoor and Mobile Radio Communications (PIMRC) 2006, Helsinki, Finland, September 2006 [2].

Thomas Zasowski was with the Communication Technology Laboratory, ETH Zurich, 8092 Zurich, Switzerland. He is now with Swisscom Strategy & Innovation, 3050 Bern, Switzerland (e-mail: thomas.zasowski@swisscom.com).

Armin Wittneben is with the Communication Technology Laboratory, ETH Zurich, 8092 Zurich, Switzerland (e-mail: wittneben@nari.ee.ethz.ch).

Digital Object Identifier 10.1109/JSAC.2009.0901xx.

model is subdivided into 3 channel models to accommodate the different receiver positions. Moreover, it is based on 144 measurements, only, which were done in a large empty room to reduce the impact of the environment. Another BAN channel model based on FDTD simulations has been presented in [10] for the frequency range from 3 to 9 GHz. Additionally, a second model combining the uniform geometrical theory of diffraction and ray tracing has been derived in the same work. For both models, only links between a central node at the hip and six nodes with different positions at the body have been considered. In [11], a similar setup has been regarded with only three nodes placed on different positions of the body and one central unit. The derivation of the channel model parameters have been based on a frequency-dependent FDTD simulation. There, the frequency range was chosen from 3.1 to 10.6 GHz. To account also for a non-centralized BAN scenario, a novel channel model based on 1100 measurements in the frequency range between 2 and 8 GHz is proposed. The measurements were done in an anechoic chamber with 11 test persons for 20 different links at the body. To account also for possible temporal variations each measurement was done 5 times. The resulting number of measurements, which the channel model is based on, is much larger compared to already other BAN channel models. From the channel measurements the power delay profile, path loss, and the distribution of the multipath amplitudes are determined. The position of devices in a non-centralized BAN is usually not known beforehand and their position may change. Hence, the model is not subdivided into channel models according to the nodes position but all measurements are considered together for a single model, which is different from other BAN channel models.

The measurements, which the UWB BAN channel model is based on, and the channel model itself are shown in Section II and Section III, respectively. In Section IV, the maximum likelihood receiver structures for PPM, TR PAM, and TR PIAM with different CSI level are presented. The performance of these receiver structures is evaluated in Section V based on the derived UWB BAN channel model followed by a comparative discussion of the receiver performance in Section VI. Finally, conclusions are given in Section VII.

II. Measurement Setup

The channel measurements were performed in an anechoic chamber with several test persons. Transfer functions were measured with a network analyzer in the frequency range between 2 and 8 GHz. Two antennas Skycross SMT-3TO10M-A [12], which were mainly chosen due to their small size and their large bandwidth, were used for these measurements. The antennas are suited for a frequency range from 3.1 to 10 GHz and have a dipole-like antenna pattern. To reduce the influence of unwanted cable effects on the measurements the antennas were mounted on glass-fiber reinforced plastic (GRP) arms on tripods as shown in [13]. The tripods were covered by absorbing material to reduce reflections caused by them. With such a measurement setup only the antennas were placed close to the test person while the cables led away from the test person as fast as possible.

Using the above described measurement setup, transfer functions were determined for 20 different links at the human body. The nodes were placed at positions where they would be located in most reasonable application scenarios are. Each measurement was repeated 5 times for 11 test persons, resulting in 55 measurements per link, i.e., 1100 measurements altogether. The repetitions were done to account also for short term effects such a slight unintentional motions of the test persons. Moreover, different measurements were done with different test persons to also average over properties of different persons, i.e. in particular over the size of the persons. To consider also the effects due to arm motions, three measurements were done with the antenna placed at the wrist, i.e., with the wrist in front of the body, besides the body, and behind the body. Thus, the following links were chosen for the measurements: on ear - on ear, behind ear - behind ear, behind ear - wrist in front, behind ear - wrist backward, behind ear - wrist laterally, behind ear - belt buckle, shoulder - belt buckle, shoulder - belly, shoulder - belly, shoulder - chest, shoulder - wrist in front, shoulder - wrist backward, shoulder - wrist laterally, belt buckle - belly, belt buckle - hip, belt buckle - back, belt buckle - knee, belt buckle - forefoot, belt buckle - heel.

III. Channel Model

In the following a simple BAN channel model is derived. Since the position of transmitter and receiver is usually not known for many BAN applications, different scenarios are not distinguished, i.e., the model is based on all measurements and not subdivided into models for different positions of the nodes. All transfer functions are transformed into complex channel impulse responses by means of an inverse Fourier transform. The energy in the channel impulse responses at the human body decays very fast. Hence, only the first 15 ns, i.e., 240 measurement samples with a sampling rate of 16 GHz, of each impulse response are considered for the modeling. These 15 ns correspond to a distance of 4.5 m in free space. Due to the size of human bodies and since measurements were done in an anechoic chamber, it can be assumed that no reflections are received after the considered time. The impulse responses are aligned such that they start at the time instant, where the first substantial increase in energy can be observed. All channel impulse responses are normalized by the path loss for each link.

a) Distribution of Channel Taps: From the measurements it can be easily seen that the distribution of the phases is uniform within $\{0, 2\pi\}$. However, the determination of the amplitude distributions requires more effort. To determine the statistical distribution of the amplitudes, the Akaike information criterion (AIC) is used [14]. The AIC, which has been used for channel modeling e.g. in [15] or [16], is based on the Kullback-Leibler (KL) distance, which can be used to determine the similarity of two different probability density functions. It is possible to write the KL distance as a difference between two statistical expectations [17] as

$$\begin{aligned} I(f,g) &= \int f(x)\log(f(x))dx - \int f(x)\log(g(x|\Theta))dx \\ &= \mathcal{E}_f[\log(f(x))] - \mathcal{E}_f[\log(g(x|\Theta))], \end{aligned} \tag{1}$$

each with respect to the real distribution f, which is given. The distribution g depends on a set of parameters Θ and should

approximate f. The KL distance is always larger than or equal to zero, i.e., $I(f,g) \geq 0$. The equality holds only if $f(x) = g(x|\Theta)$. The first term $\mathcal{E}_f[\log(f(x))]$ is not known, because it depends on the true distribution but it can be regarded as a constant. Hence, (1) can be written as

$$I(f,g) - C = -\mathcal{E}_f[\log(g(x|\Theta))]. \tag{2}$$

The term $I(f,g) - C$ is regarded as a relative distance between f and g. Thus, it is sufficient to consider only $\mathcal{E}_f[\log(g(x|\Theta))]$ for calculation of a relative distance. Defining the best fitting model, $\mathcal{E}_f[\log(g(x|\Theta))]$ has to be maximized because $I(f,g) \geq 0$. It is shown in [18] that for an infinite large number of observations N

$$\begin{aligned}\lim_{N\to\infty} \frac{1}{N}\sum_{n=1}^{N} \log(g(x_n|\Theta)) &= \int f(x)\log(g(x|\Theta))dx \\ &= \mathcal{E}_f[\log(g(x|\Theta))]\end{aligned} \tag{3}$$

and that maximizing $\frac{1}{N}\sum_{n=1}^{N}\log(g(x_n|\Theta))$ with respect to Θ yields the maximum likelihood estimate $\hat{\Theta}$, i.e.,

$$\hat{\Theta} = \arg\max_{\Theta}\left[\frac{1}{N}\sum_{n=1}^{N}\log(g(x_n|\Theta))\right]. \tag{4}$$

Using (4), Akaike defined its information criterion [14] as

$$AIC = -\frac{2}{N}\sum_{n=1}^{N}\log(g(x|\hat{\Theta})) + 2K, \tag{5}$$

where K denotes the number of estimable parameters and the AIC is regarded as an estimate for the approximation quality of different distributions. The log-likelihood $\frac{1}{N}\sum_{n=1}^{N}\log(g(x|\hat{\Theta}))$ is asymptotically biased. With the simple expression K as an estimator of $\frac{1}{N}\sum_{n=1}^{N}\log(g(x|\hat{\Theta}))$ for the asymptotic bias an approximately unbiased estimator is achieved. A more intuitive explanation of the AIC is as follows. $I(f,g)$ can be decreased by using additional known parameters for the approximation g, because g can be chosen closer to f for a fixed parameter set. Since these additional parameters are usually not known but have to be estimated, further uncertainty is added to the estimation of $I(f,g)$. Hence at a certain point, adding still more parameters has a negative effect. The Kullback-Leibler distance $I(f,g)$ will increase due to noise in the estimated parameters that are not necessary to achieve a good model. This effect is considered in the AIC. While $\frac{1}{N}\sum_{n=1}^{N}\log(g(x|\hat{\Theta}))$ decreases, K increases with additional number of parameters. Thus, models with a high number of parameters are penalized. To rank different distributions, the AIC differences

$$\Phi_j = AIC_j - AIC_{\min} \tag{6}$$

are used [17]. AIC_j denotes the AIC value of the j^{th} distribution and $AIC_{\min}$ denotes the minimum AIC indicating the distribution with the best fit. The likelihood of a model g_j with given data is computed by

$$\mathcal{L}(g_j|x) \propto e^{-\frac{1}{2}\Phi_j}. \tag{7}$$

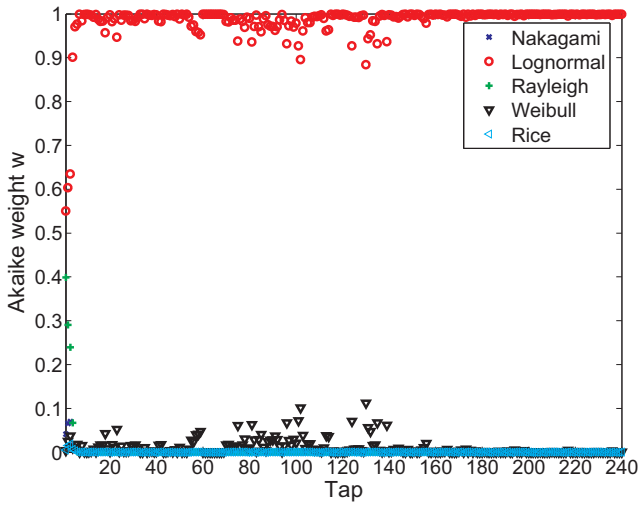

Fig. 1. Akaike weights for the body area network channel plotted versus the corresponding channel tap

The likelihood values for the different models are used to calculate the Akaike weights [19]

$$w_j = \frac{e^{-\frac{1}{2}\Phi_j}}{\sum_{i=1}^{J} e^{-\frac{1}{2}\Phi_i}} \tag{8}$$

which satisfy $\sum_{j=1}^{J} w_j = 1$. The weight w_j is an estimate of the relative likelihood that a distribution is the best fit to the true data within a candidate set. Hence, the Akaike weights give besides the selection of the best candidate also information on the relative approximation quality.

For determination of the amplitude distributions of the measured channel impulse responses frequently used distribution functions in UWB channel modeling [20] are used, i.e., Nakagami, Rice, Lognormal, Weibull, and Rayleigh distribution. While the first 4 distributions depend on 2 parameters, i.e., $K = 2$, the Rayleigh distribution depends on 1 parameter only.

In Fig. 1, the Akaike weights of the different distributions are plotted. It can be observed that Rice and Nakagami distribution have only very small weights, i.e., it is very unlikely that the amplitudes are distributed according to these distributions. Although the weights for the Rayleigh and the Weibull distribution are slightly larger, they are also small compared to the Akaike weights for the lognormal distribution. Therefore, it is assumed that the amplitudes are lognormal distributed according to

$$f(x) = \frac{1}{\sigma_x\sqrt{2\pi}} e^{-\frac{(\ln(x)-\mu)^2}{2\sigma_x^2}}, \tag{9}$$

since these Akaike weights are in general the highest, i.e., the lognormal distribution is the most likely one.

To verify the assumption that the channel taps are lognormal distributed the cumulative distribution functions (cdf) of the measurements are compared to theoretical ones. The parameters for the theoretical curves are determined by a maximum likelihood estimation. In Fig. 2, the cdfs are shown for one exemplarily chosen channel tap. It can be seen that neither the cdfs for Rayleigh, Rice, Weibull nor Nakagami

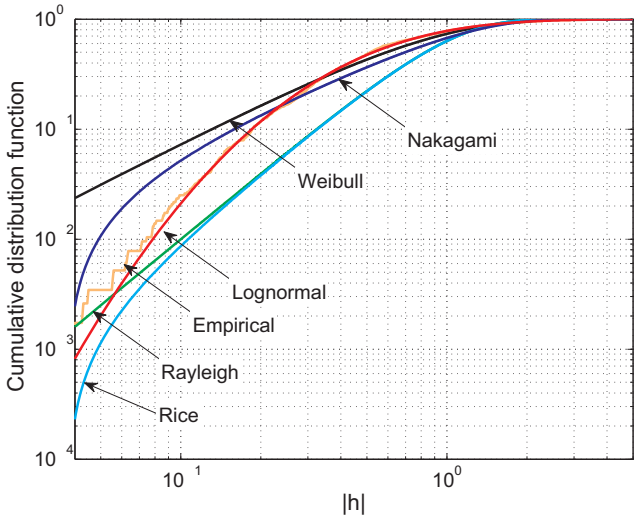

Fig. 2. Cumulative distribution functions for an exemplarily chosen channel tap

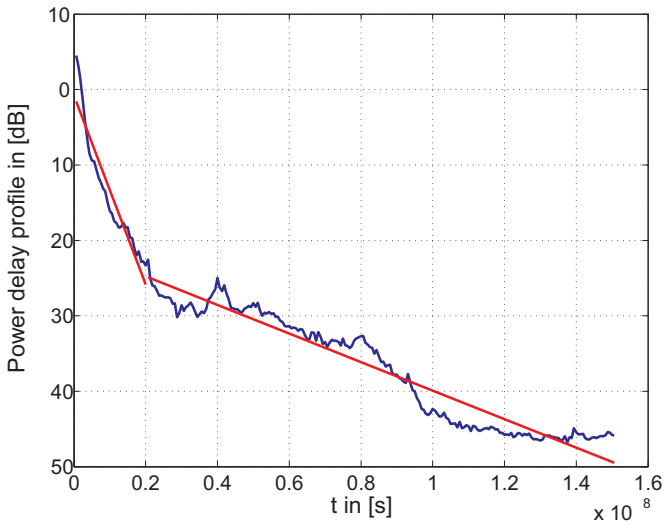

Fig. 3. Power delay profile over all channel measurements and approximation of the APDP based on (10) and (11)

distribution fit the measured distribution well. However, the lognormal distribution fits the measured cdf very well over the whole range of values verifying the result of the AIC method. This observation corresponds with the results in [16] and [21] where also a lognormal amplitude distribution was determined for BAN channels.

The parameters μ and σ_x for the lognormal distribution in (9) are determined by a maximum likelihood estimation and averaged over all normalized channel taps as $\mu = -0.60$ and $\sigma_x = 0.84$.

b) Power Delay Profile and Path Loss: Besides the distribution of the channel taps also the power delay profile and the path loss are of interest. The power delay profile (PDP), averaged over all channel measurements, is shown in Fig. 3. A decay over the time can be observed from this plot. Since the PDP does not show a linear decay in the logarithmic domain over the considered dynamic range, a function that approximates the power delay profile has to be defined for the model. From Fig. 3 two ranges with different linear decays can be observed. Up to about 2 ns the PDP is decaying relatively steep. For delays above about 2 ns the linear decay gets flatter. This flattening is caused by effects such as reflections from the body or also from the environment. Although the measurements were done in an anechoic chamber, in particular, the absorbing material placed on the tripods is only attenuating the waves by about 15 dB and can still cause reflections which are strongly attenuated.

Due to this behavior of the PDP in logarithmic scale the PDP shown in Fig. 3 is approximated by two exponentials for the different ranges. The approximation for the range up to 2 ns is given by

$$A = a_1 - a_2 \cdot t \tag{10}$$

and for the range above 2 ns by

$$B = b_1 - b_2 \cdot t, \tag{11}$$

where t denotes the time in seconds. The parameters a_1, a_2, b_1, b_2 are determined as $a_1 = -0.8$, $a_2 = 12.5 \cdot 10^{-9}$,

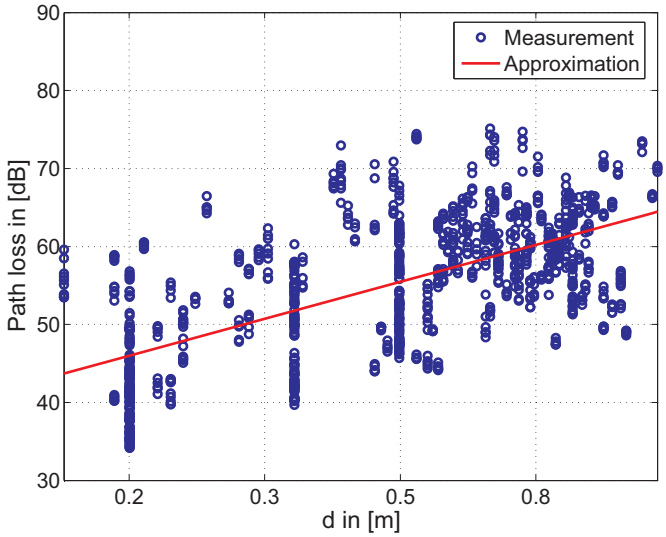

Fig. 4. Measured and approximated path loss for the body area network channel

$b_1 = -21.0$, and $b_2 = 1.9 \cdot 10^{-9}$ using a least square curve fitting in the logarithmic domain. From the APDP it can be concluded that the main energy is contained in a very short time interval. Only about 2 ns after the maximum peak the energy is decreased by about 40 dB.

The path loss (PL) can be calculated directly from the measured frequency transfer functions [22]. If there are M transfer functions available for a distance d with N frequency points, the average path loss is given by

$$\mathrm{Pl}(d) = \frac{1}{MN} \sum_{i=1}^{N} \sum_{j=1}^{M} \left| H_j^{(d)}(f_i) \right|^2 . \tag{12}$$

$H_j^{(d)}(f_i)$ denotes the j^{th} frequency transfer function at a frequency f_i at a distance d. The distance d is the distance between transmitter and receiver on the surface of the body. Assuming $\mathrm{PL}(d) \propto d^{\gamma}$ the path loss exponent γ can be

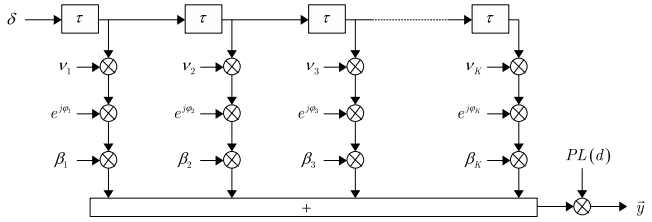

Fig. 5. Tap delay line representation of the channel model

evaluated at any distance d as described in [23] by

$$\mathrm{PL}(d) = \mathrm{PL}_0 + 10 \cdot \gamma \cdot \log_{10}\left(\frac{d}{d_0}\right) + S_\sigma \qquad (13)$$

where PL_0 denotes the path loss at a distance d_0. d_0 is set to $d_0 = 0.1$ m and S_σ is a lognormal variable with standard deviation σ_S, which accounts for the path loss variations at a fixed distance. To determine the path loss $\mathrm{PL}(d)$, which includes in this case attenuation, reflection, and diffraction effects, a least square fit computation is performed yielding a reference path loss

$$\mathrm{PL}_0 = 38.9 \text{ dB} \qquad (14)$$

and a path loss exponent

$$\gamma = 2.4. \qquad (15)$$

The standard deviation σ_S of the lognormal distributed variable S_σ is determined as

$$\sigma_S = 6.8 \text{ dB} \qquad (16)$$

using a maximum likelihood estimation. In Fig. 4, the measured path losses $\mathrm{Pl}(d)$ are displayed as circles for the different distances d, while the approximation $\mathrm{PL}(d)$ is shown as line. It can be observed that the path loss is varying over a wide range for similar distances d. These variations are mainly caused by the fact that there exist several measurements with similar distances for different links and different persons. The determined reference path loss in (14) is close to the one given in the IEEE 802.15.4a standard [8]. However, the shown path losses at larger distances are higher than the ones which we measured. This difference might have several reasons as e.g. the considered antenna type or the fact that the results in [21] are based on FTDT simulations. Channel investigations based on measurements are shown in [24], where the impact of the antenna on the path loss and the path loss exponent is shown. Performing channel measurements in the frequency range between 3 and 9 GHz, the authors calculate reference path loss of 86.5dB and 70.3dB at 1m distance depending on the antenna type and path loss exponents of 4.4 and 2.7, respectively. These parameters are close to the ones which we got with our measurements.

Using the above determined parameters channel impulse responses can be generated according to the tap delay line representation of the channel model in Fig. 5. For each tap of the impulse response the impulse δ is delayed by $\tau = 62.5$ ps. In each branch the impulse is multiplied by the lognormal magnitude $\nu_i \sim \mathcal{LN}\{-0.60, 0.84\}$ and the exponent $e^{j\phi_i}$ with phase ϕ_i equally distributed in $\{0, 2\pi\}$. According to

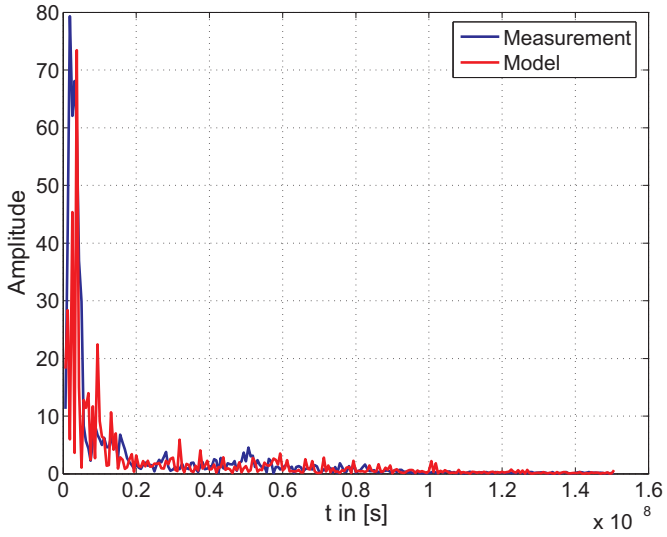

Fig. 6. Exemplary absolute values of the measured and modeled complex channel impulse responses

the delay of the channel tap, afterwards a multiplication with the corresponding linear value β_i of the power delay profile is done calculated from (10) and (11). Finally, all taps are summed up and multiplied with the distance dependent path loss $\mathrm{PL}(d)$ given in (13) yielding the modeled channel impulse response vector $\vec{y}$.

Exemplarily, a measured and a modeled channel impulse response are shown in Fig. 6. It can be seen that both impulse responses show a similar behavior. After a strong peak at the beginning both impulse responses exhibit a very fast decay.

IV. Receiver Structures

Due to their complexity coherent receivers are not suited for the use in a BAN. Therefore, for this kind of applications simple receiver concepts such as transmitted-reference receiver or energy detector are very promising alternatives. In the following, symbol-wise maximum-likelihood receiver structures are presented for PPM, TR PAM, and TR PIAM with partial CSI. Due to complexity reasons only the assumption of APDP knowledge or no CSI are reasonable. However, the ML receivers with full CSI are given for comparison reason. It is assumed that only one pulse is transmitted per symbol, which is a reasonable assumption for short range communication in wireless body area networks due to the moderate path loss. Moreover, for the derivation it is assumed that the delay spread is small compared to one half-frame of duration $T/2$, i.e, there is no intersymbol interference (ISI).

A. Binary Pulse Position Modulation

Using binary pulse position modulation (PPM), data is modulated in the pulse position as shown in Fig. 7. Hence, the sampled receive signal in the considered PPM frame is given by

$$\vec{r}_1 = \frac{1}{2}(1 - a_1)\vec{h} + \vec{n}_1 \qquad (17)$$

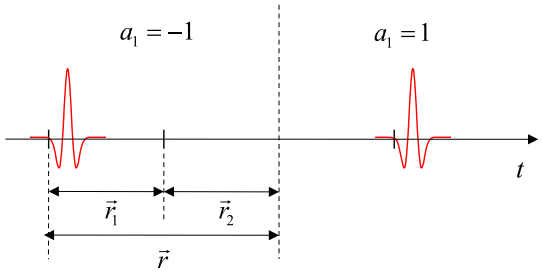

Fig. 7. Transmit pulse constellations for PPM

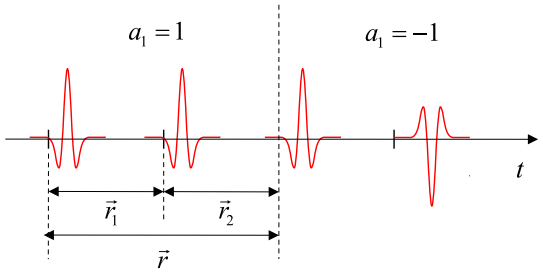

Fig. 8. Transmit pulse constellations for TR PAM

for the first half frame and

$$\vec{r}_2 = \frac{1}{2}(1 + a_1)\vec{h} + \vec{n}_2 \tag{18}$$

for the second half frame, depending on the transmit symbol $a_1 \in \{\pm 1\}$ in the present PPM frame. $\vec{h}$ denotes the CIR. In the remainder, we assume that the taps of the CIR are statistically independent normal random variables with zero mean. $\vec{n}_1$ and $\vec{n}_2$ contain the additive white Gaussian noise (AWGN), both with variance σ^2. Since $\vec{r}_1$ and $\vec{r}_2$ are not overlapping, the whole receive signal in the considered PPM frame can be described by

$$\vec{r} = [\vec{r}_1, \vec{r}_2] = \frac{1}{2}[(1 - a_1)\vec{h}_1 + (1 + a_1)\vec{h}_2 + \vec{n}] \tag{19}$$

with

$$\vec{h}_1 = [\vec{h}, 0, \ldots, 0] \qquad \vec{h}_2 = [0, \ldots, 0, \vec{h}] \tag{20}$$

and

$$\vec{n} = [\vec{n}_1, \vec{n}_2]. \tag{21}$$

Both, $\vec{r}_1$ and $\vec{r}_2$ contain $N/2$ elements, i.e., $\vec{r}$ contains N elements.

The receiver with full CSI is given by

$$L = \frac{1}{\sigma^2} \sum_{k=1}^{N/2} \left(r_{k+N/2} h_k - r_k h_k \right), \tag{22}$$

where the receive signal is correlated with a template and thus the channel taps are coherently combined.

Assuming the knowledge of the APDP the receiver knows the correlation matrix of $\vec{h}$, i.e.,

$$\Lambda_{hh} = \begin{bmatrix} \mathcal{E}[h_1^2] & \ldots & 0 \\ \vdots & \ddots & \vdots \\ 0 & \ldots & \mathcal{E}[h_{N/2}^2] \end{bmatrix} = \begin{bmatrix} \lambda_{h,1} & \ldots & 0 \\ \vdots & \ddots & \vdots \\ 0 & \ldots & \lambda_{h,N/2} \end{bmatrix}. \tag{23}$$

As shown in [25] and [1], in this case the log-likelihood ratio is given by

$$L = \frac{1}{2\sigma^2} \sum_{k=1}^{N/2} \frac{r_{k+N/2}^2 - r_k^2}{1 + \frac{\sigma^2}{\lambda_{h,k}}}, \tag{24}$$

i.e., this is a typical energy detector, whose output is weighted with the APDP. Channel taps that are in average small are considered for decision less than large ones.

A receiver knowing just the average energy of the CIR and the noise variance σ^2 can be regarded as a special case of the receiver with APDP knowledge. Since the channel taps are not known, all diagonal elements of (23) are assumed to be equal. Inserting this into (24) yields the common energy detector

$$L \propto \sum_{k=1}^{N/2} r_{k+N/2}^2 - r_k^2. \tag{25}$$

B. Transmitted Reference Pulse Amplitude Modulation

Next, the optimum receiver for transmitted reference pulse amplitude modulation (TR PAM) is derived. In TR systems, a doublet consisting of two pulses is transmitted as it can be seen in Fig. 8. Usually, the first pulse is a reference, which serves as noisy correlation template at the receiver, while the second pulse contains the data. The reference signal is assumed to be always positive while the sign of the data pulse is determined by the transmit symbol $a_1 \in \{\pm 1\}$. Hence the sampled receive signal in the considered time frame is given by

$$\vec{r}_1 = \vec{h} + \vec{n}_1 \tag{26}$$

for the first half frame and

$$\vec{r}_2 = a_1\vec{h} + \vec{n}_2 \tag{27}$$

for the second half frame. As in the previous section, the whole receive signal in the considered frame can be described by

$$\vec{r} = [\vec{r}_1, \vec{r}_2] = \vec{h}_1 + a_1\vec{h}_2 + \vec{n}. \tag{28}$$

Both, $\vec{r}_1$ and $\vec{r}_2$ contain $N/2$ elements, i.e., $\vec{r}$ contains N elements.

The receiver for TR PAM with full CSI is given by

$$L = \frac{1}{\sigma^2} \sum_{k=1}^{N/2} \left(2 r_{k+N/2} h_k \right) \tag{29}$$

which is just the correlation of data pulse and template. The reference pulse is not considered for decision and yields just a performance degradation due to the energy required for its transmission.

As for the binary PPM the receiver knows the correlation matrix (23) in case of APDP knowledge. Then the log-likelihood ratio is given by

$$L = \frac{1}{\sigma^2} \sum_{k=1}^{N/2} \frac{r_k r_{k+N/2}}{2 + \frac{\sigma^2}{\lambda_k}} \tag{30}$$

as presented in [2]. This decision rule corresponds to the classical TR receiver in [6] extended by a weighting with the noise variance and the average energy of the k^{th} channel

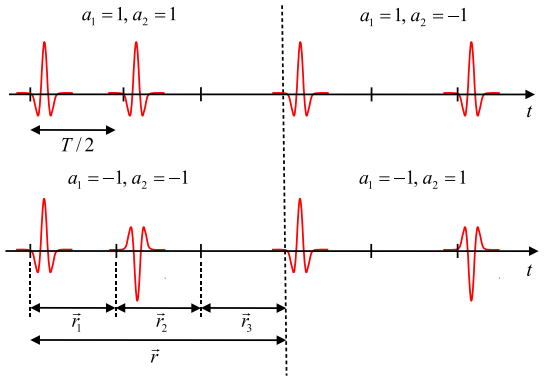

Fig. 9. Transmit pulse constellations for TR PIAM

tap. If the noise variance σ_n^2 is large compared to λ_k^2, the multiplication of reference and data signal for the k^{th} channel tap does not contribute to L.

Considering again the receiver which only knows the average energy of the CIR and the noise variance σ^2, the ML receiver from (30) reduces to the typical TR PAM correlation receiver, i.e.,

$$L \propto \sum_{k=1}^{N/2} r_k r_{k+N/2}. \tag{31}$$

C. Transmitted Reference Pulse Interval Amplitude Modulation

In the previous sections ML receivers for binary PPM and TR PAM were derived. In the following both modulation schemes are combined to one modulation scheme, which is referred to as transmitted reference pulse interval amplitude modulation (TR PIAM) [7]. In contrast to the typical TR scheme, where information is contained only in the amplitude, the information is contained in the pulse position, too, as shown in Fig. 9. In the following, it is assumed that the reference pulse is always positive while the sign and the position of the data pulse are determined by the transmit symbol. Thus, the sampled receive signal in the first time frame is given by

$$\vec{r}_1 = \vec{h} + \vec{n}_1, \tag{32}$$

in the second time frame

$$\vec{r}_2 = \frac{1}{2}(a_1 + a_2)\vec{h} + \vec{n}_2, \tag{33}$$

and in the third time frame

$$\vec{r}_3 = \frac{1}{2}(a_1 - a_2)\vec{h} + \vec{n}_3. \tag{34}$$

The data symbols are $a_1, a_2 \in \{\pm 1\}$ and $\vec{h}$ denotes the channel impulse response. It is assumed that the taps of the CIR are statistically independent normal random variables with zero mean. $\vec{n}_1$, $\vec{n}_2$ and $\vec{n}_3$ contain the AWGN, all with variance σ^2. The whole receive signal over the three time slots is given by

$$\begin{aligned}\vec{r} =& [\vec{r}_1, \vec{r}_2, \vec{r}_3] \\ =& \vec{h}_1 + \frac{1}{2}(a_1 + a_2)\vec{h}_2 + \frac{1}{2}(a_1 - a_2)\vec{h}_3 + \vec{n}\end{aligned} \tag{35}$$

with

$$\begin{aligned}\vec{h}_1 &= [\vec{h}, 0, \ldots, 0], \\ \vec{h}_2 &= [0, \ldots, 0, \vec{h}, 0, \ldots, 0], \\ \vec{h}_3 &= [0, \ldots, 0, \vec{h}]\end{aligned} \tag{36}$$

and

$$\vec{n} = [\vec{n}_1, \vec{n}_2, \vec{n}_3]. \tag{37}$$

$\vec{r}_1$, $\vec{r}_2$, and $\vec{r}_3$ contain $N/2$ elements each, i.e., $\vec{r}$ contains $\frac{3}{2}N$ elements.

For the TR PIAM there exist four hypotheses for decision. Hence, the maximum likelihood receiver is now described by

$$[\hat{a}_1 = \hat{\imath}, \hat{a}_2 = \hat{\jmath}] = \arg\max_{i,j} \ln(p_{i,j}). \tag{38}$$

In case of full CSI, the likelihoods in (38) are given by

$$\ln\left(p_{1,1}\right) \propto \sum_{k=1}^{N/2} \frac{r_{k+N/2} h_k}{\sigma^2}, \tag{39}$$

$$\ln\left(p_{1,-1}\right) \propto \sum_{k=1}^{N/2} \frac{r_{k+N} h_k}{\sigma^2}, \tag{40}$$

$$\ln\left(p_{-1,1}\right) \propto \sum_{k=1}^{N/2} \frac{-r_{k+N} h_k}{\sigma^2}, \tag{41}$$

$$\ln\left(p_{-1,-1}\right) \propto \sum_{k=1}^{N/2} \frac{-r_{k+N/2} h_k}{\sigma^2}. \tag{42}$$

The expressions in (39) to (42) are the correlations of a template with either the receive signal in the first time slot or in the second time slot. Assuming again the knowledge of the channel correlation matrix, the likelihoods $p_{i,j}$ for the different hypotheses in (38) are given by

$$\ln(p_{1,1}) = \frac{1}{2\sigma^2} \sum_{k=1}^{N/2} \frac{2 r_k r_{k+N/2} - r_{k+N}^2}{2 + \frac{\sigma^2}{\lambda_{h,k}}}, \tag{43}$$

$$\ln(p_{1,-1}) = \frac{1}{2\sigma^2} \sum_{k=1}^{N/2} \frac{2 r_k r_{k+N} - r_{k+N/2}^2}{2 + \frac{\sigma^2}{\lambda_{h,k}}}, \tag{44}$$

$$\ln(p_{-1,1}) = \frac{1}{2\sigma^2} \sum_{k=1}^{N/2} \frac{-2 r_k r_{k+N} - r_{k+N/2}^2}{2 + \frac{\sigma^2}{\lambda_{h,k}}}, \tag{45}$$

$$\ln(p_{-1,-1}) = \frac{1}{2\sigma^2} \sum_{k=1}^{N/2} \frac{-2 r_k r_{k+N/2} - r_{k+N}^2}{2 + \frac{\sigma^2}{\lambda_{h,k}}}. \tag{46}$$

From (43) to (46) it can be observed that the first term in the numerator tends towards 0 for the effectively transmitted symbols while all other terms are growing.

For the receiver which only knows the average energy of the CIR and the noise variance σ^2, the likelihoods that have

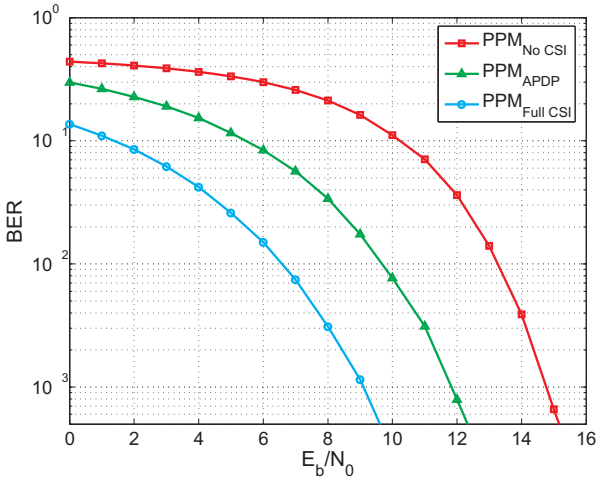

Fig. 10. Bit error ratios for binary PPM

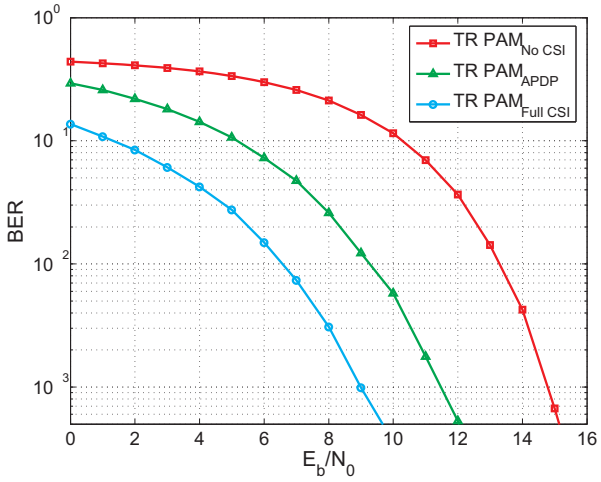

Fig. 11. Bit error ratios for transmitted reference PAM

to be inserted in (38) are given by

$$\ln(p_{1,1}) \propto \sum_{k=1}^{N/2} 2r_k r_{k+N/2} - r_{k+N}^2, \tag{47}$$

$$\ln(p_{1,-1}) \propto \sum_{k=1}^{N/2} 2r_k r_{k+N/2} - r_{k+N/2}^2, \tag{48}$$

$$\ln(p_{-1,1}) \propto \sum_{k=1}^{N/2} -2r_k r_{k+N} - r_{k+N/2}^2, \tag{49}$$

$$\ln(p_{-1,-1}) \propto \sum_{k=1}^{N/2} -2r_k r_{k+N/2} - r_{k+N}^2. \tag{50}$$

These likelihoods show that the resulting ML receiver for TR PIAM is a combination of an energy detector and a transmitted reference receiver in case of no CSI. The complexity of the derived ML receiver is mainly increased by the two required delays. However, from realization point of view only one delay is sufficient if the reference pulse is located in the middle of the possible data pulse positions.

V. Performance Evaluation

In the previous sections the maximum likelihood receiver structures for binary PPM, TR PAM, and TR PIAM have been derived assuming no channel state information or APDP knowledge. These receiver structures are compared by means of bit error simulations in the following. The BERs are plotted over the signal-to-noise ratio E_b/N_0, where E_b denotes the energy per bit and $N_0/2$ is the noise power spectral density. As in [3] a medium data rate of 500 kbps and a 1 % duty cycle are desired yielding a peak data rate of 50 Mbps. Thus, one frame has a duration of 20 ns. The integration time has the duration of one half frame, i.e., 10 ns. The TR PIAM requires three half frames for transmission of two bits. For comparison reasons the duration of a half frame and the integration time are the same as for PPM and TR PAM. However, this choice results in a data rate of 666 kbps for the TR PIAM scheme. The performance evaluation presented in the following is based on the previously presented BAN channel model.

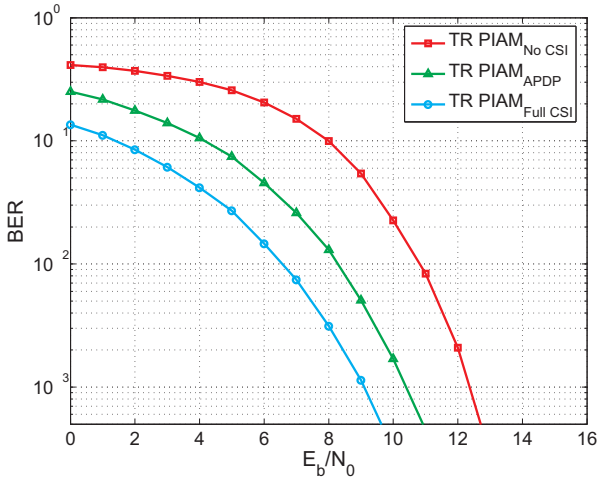

Fig. 12. Bit error ratios for transmitted reference PIAM

In Fig. 10 the BER curves for binary PPM are shown for the different receiver structures. The receiver with APDP knowledge uses this information to integrate only over the large taps of the CIR and blanks the small taps. Hence, the performance improves compared to the energy detector and is only about 2 dB worse than with full CSI.

The BER curves for the transmitted reference PAM receivers are shown in Fig. 11. The performance equality of the transmitted reference receiver and the energy detector, i.e, the receiver structures without CSI, is shown in [26]. However, from the BER curves in Fig. 10 and Fig. 11 it can be seen that this equality is also given for the receiver structures which have full CSI or which know the APDP.

Compared to the binary PPM and the TR PAM, the derived TR PIAM receivers have better BER performance in case of limited CSI as it can be seen in Fig. 12. Only the coherent receiver shows the same performance as the coherent receivers for binary PPM and TR PAM. The TR PIAM receivers are about 1-2 dB better than the corresponding TR PAM and PPM receivers.

In general, the receivers with APDP knowledge are very attractive since they yield a good compromise between per-

formance and complexity. Their performance is substantially better than the performance of the receivers without CSI. However, the acquisition of the APDP knowledge is much simpler than the full channel estimation required by the matched filter receivers.

Although the measurements for the model were done in an anechoic chamber, this model can be also considered for scenarios where no obstacles are in close vicinity of the body such as in outdoor scenarios. Of course in scenarios with obstacles close to the body additional multipaths occur in the CIR. However, the parts of the CIR caused by transmission around the body remain unchanged while additional delayed paths caused by the environment are added as it can be seen in [13]. Position and attenuation of these additional paths depend mainly on the environment but also on other parameters as, e.g., antenna orientation. Considering a system with the same data rate, i.e, the same frame duration, ISI might be introduced by the additional multipaths. Since symbol-wise ISI-aware receiver structures as presented in [1] and [2] are too complex for the use in a BAN, the frame durations have to be increased to reduce the amount of ISI and to allow for usage of the presented receiver structures. In such a case the additional multipaths can also be considered for decision and the performance of the receivers with APDP knowledge gets better. For the receivers without CSI also the effect of collecting more noise due to longer integration windows has to be considered. Hence, performance does not necessarily has to get better by considering the additional multipath components.

VI. Discussion of the Performance Results

From Fig. 10 to Fig. 12 it can be seen that all three receiver structures with full CSI knowledge show the same bit error performance. In the case of full CSI, coherent detection is possible and the performance of the receiver structures is determined by the minimum distances between the different symbols. The signal space representations and the minimum distances for the three modulation schemes are presented in Fig. 13. Assuming an energy per bit E_b the minimum distance between the two possible symbols is given by the distance of the data pulses $d_{min} = \sqrt{2E_b}$. Using transmitted reference PAM, which is an antipodal modulation scheme, the energy per bit E_b for decision is reduced by a factor of 2, because the reference pulse does not contain any information. Hence, the minimum distance is also given by $d_{min} = \sqrt{2E_b}$. The energy loss due to the reference pulse is compensated in TR PIAM by the transmission of two bits per symbol. Due to the combination of orthogonal and antipodal modulation the signal space representation is also a combination of the corresponding signal space representations. Assuming an energy per bit E_b the minimum distance for TR PIAM is also $d_{min} = \sqrt{2E_b}$. This result verifies the same performance of the coherent receivers for the three different modulation schemes.

The ML estimators in the case of APDP knowledge are given in (24), (30), and (38) for binary PPM, TR PAM, and TR PIAM, respectively. From the equations it can be observed that a weighting with the average channel tap amplitude is done by these receiver structures. If the average channel tap amplitude λ_k is small compared to the noise variance σ^2, the corresponding receive signal tap is not considered for decision. The performance for binary PPM and TR PAM is the same since the bit energy, which is reduced by a factor of 2, has to be considered again for TR PAM. However, the distance between the two possible symbols is the same. For TR PIAM the distance is larger, since the energy per bit is the same as for binary PPM. However, the performance gain of TR PIAM is less than 3 dB compared to the both other modulation schemes, since noise from three instead of two time slots has to be considered for the TR PIAM ML decision.

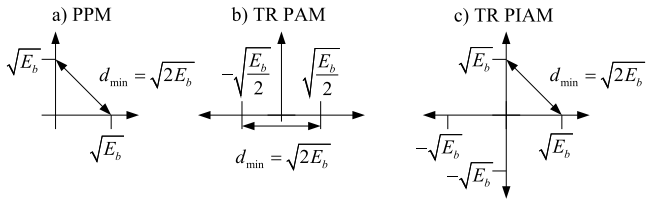

Fig. 13. Signal space representations and minimum distances for the different modulation schemes

In [26], it has been shown that in the case of no CSI the performance for binary PPM and TR PAM is the same. There, it has been shown by using a Gaussian approximation of the noise that the decision SNR for both receiver structures is the same and hence yields the same performance. Alike in the previous cases, the TR PIAM modulation scheme does not exhibit the E_b penalty of the TR PAM receiver. However, the presence of noise in three instead of two time slots has to be considered here, too. The performance of the three receiver structures without CSI mainly depends on the integration time. If the integration time is longer than the part of the channel containing the substantial part of the energy, mainly noise is collected during this additional integration time. However, integration time which is too short results in omitting a substantial part of the energy that would improve the performance. Hence, there exists an optimum integration time (cf. [26]).

In contrast to the presented PPM receivers, the TR PAM and TR PIAM receivers require an analog delay line, which is difficult to realize in integrated systems. A simpler digital delay line is not suited for a BAN due to the high sampling rate necessary in fully digital UWB receivers. From complexity and performance point of view, the most interesting receiver structures for BANs are based on PPM. Not requiring a delay line the performance is the same as for the corresponding TR PAM receivers. In the case that a delay line can be afforded, TR PIAM should be preferred to TR PAM because of a better performance with similar complexity.

VII. Conclusions

Based on 1100 measurements with several test persons a simple channel model for UWB BAN was derived. The measurements were done in an anechoic chamber in the frequency band between 2 and 8 GHz. Power delay profile, path loss, and the distribution of the multipath amplitudes were determined. Using the novel channel model, performance of PPM, TR PAM, and TR PIAM receiver structures with different level of CSI was evaluated. Assuming the knowledge of the average

power delay profile, the maximum likelihood decision rules were presented. It was shown that the performance of the coherent receivers for the three different modulation formats is the same. Assuming no CSI and the knowledge of the APDP, the TR PIAM receivers outperform the corresponding PPM and TR PAM receivers. However, in all three cases the performance of the receivers with APDP knowledge improves substantially compared to the receivers without CSI. This is due to the implicit choice of the optimum integration time. Hence, receivers with APDP knowledge are a good choice for the use in UWB BAN since they are a good compromise between performance and complexity.

REFERENCES

[1] T. Zasowski, F. Troesch, and A. Wittneben, "Partial channel state information and intersymbol interference in low complexity UWB PPM detection," *IEEE International Conference on Ultra-Wideband, ICUWB 2006*, pp. 369–374, September 2006.

[2] T. Zasowski and A. Wittneben, "UWB transmitted reference receivers in the presence of co-channel interference," *The 17th Annual IEEE International Symposium on Personal, Indoor and Mobile Radio Communications, PIMRC*, September 2006.

[3] F. Troesch, C. Steiner, T. Zasowski, T. Burger, and A. Wittneben, "Hardware aware optimization of an ultra low power UWB communication system," *IEEE International Conference on Ultra-Wideband, ICUWB 2007*, pp. 174–179, September 2007.

[4] T. Zasowski, F. Althaus, M. Stäger, A. Wittneben, and G. Tröster, "UWB for noninvasive wireless body area networks: Channel measurements and results," *IEEE Conference on Ultra Wideband Systems and Technologies, UWBST*, pp. 285–289, November 2003.

[5] M. Weisenhorn and W. Hirt, "Robust noncoherent receiver exploiting UWB channel properties," *International Workshop on Ultra Wideband Systems joint with Conference on Ultrawideband Systems and Technologies, Joint UWBST & IWUWBS*, pp. 156–160, May 2004.

[6] R. Hoctor and H. Tomlinson, "Delay-hopped transmitted-reference RF communications," *IEEE Conference on Ultra Wide Band Systems and Technologies, UWBST*, pp. 265–269, May 2002.

[7] T. Zasowski, F. Althaus, and A. Wittneben, "An energy efficient transmitted-reference scheme for ultra wideband communications," *International Workshop on Ultra Wideband Systems joint with Conference on Ultrawideband Systems and Technologies, Joint UWBST & IWUWBS*, pp. 146–150, May 2004.

[8] A. F. Molisch, K. Balakrishnan, C.-C. Chong, S. Emami, A. Fort, J. Karedal, J. Kunisch, H. Schantz, U. Schuster, and K. Siwiak, "IEEE 802.15.4a channel model - final report," IEEE P802.15 02/490r1–SG3a, Tech. Rep., September 2004.

[9] A. Fort, J. Ryckaert, C. Desset, P. D. Doncker, P. Wambacq, and L. V. Biesen, "Ultra-wideband channel model for communication around the human body," *IEEE Journal on Selected Areas in Communications*, vol. 24, no. 4, pp. 927–933, April 2006.

[10] Y. Zhao, Y. Ho, A. Alomainy, and C. Parini, "UWB on-body radio channel modeling using ray theory and subband FDTD method," *IEEE Transactions on Microwave Theory and Techniques*, vol. 54, no. 4, pp. 1827–1835, April 2006.

[11] T. Tayamachi, Q. Wang, and J. Wang, "Transmission characteristic analysis for UWB body area communications," *International Symposium on Electromagnetic Compatibility, (EMC 2007)*, pp. 75–78, October 2007.

[12] Skycross SMT-3TO10M, 3.1-10 GHz Ultra-Wideband Antenna, [Online]. Available: http://www.skycross.com/Products/PDFs/SMT-3TO10M-A.pdf, March 05, 2007.

[13] T. Zasowski, G. Meyer, F. Althaus, and A. Wittneben, "UWB signal propagation at the human head," *IEEE Transactions on Microwave Theory and Techniques*, vol. 54, no. 4, pp. 1846–1857, April 2006.

[14] H. Akaike, "Information theory and an extension of the maximum likelihood principle," *Proceedings of the International Symposium on Information Theory*, pp. 267–281, 1973.

[15] U. G. Schuster, H. Boelcskei, and G. Durisi, "Ultra-wideband channel modeling on the basis of information-theoretic criteria," *IEEE International Symposium on Information Theory, ISIT*, pp. 97–101, September 2005.

[16] A. Fort, C. Desset, P. D. Doncker, P. Wambacq, and L. V. Biesen, "An ultra-wideband body area propagation channel model- from statistics to implementation," *IEEE Transactions on Microwave Theory and Techniques*, vol. 54, no. 4, pp. 1820–1826, April 2006.

[17] K. P. Burnham and D. R. Anderson, *Model Selection and Multimodel Interference: A Practical Informaion-Theoretic Approach*, 2nd ed. Springer-Verlag, 2002.

[18] H. Akaike, "A new look at the statistical model identification," *IEEE Transactions on Automatic Control*, vol. 19, no. 6, pp. 716–723, December 1974.

[19] ——, "On the likelihood of a time series model," *The Statistician*, vol. 27, no. 3/4, pp. 217–235, September - December 1978.

[20] A. F. Molisch, "Ultrawideband propagation channels-theory, measurement, and modeling," *IEEE Transactions on Vehicular Technology*, vol. 54, pp. 1528–1545, September 2005.

[21] A. F. Molisch, D. Cassioli, C.-C. Chong, S. Emami, A. Fort, B. Kannan, J. Karedal, J. Kunisch, H. G. Schantz, K. Siwiak, and M. Z. Win, "A comprehensive standardized model for ultrawideband propagation channels," *IEEE Transactions on Antennas and Propagation*, vol. 54, no. 11, pp. 3151–3166, November 2006.

[22] S. S. Ghassemzadeh, R. Jana, C. W. Rice, W. Turin, and V. Tarokh, "A statistical path loss model for in-home UWB channels," *IEEE Conference on Ultra Wideband Systems and Technologies, UWBST*, pp. 59–64, May 2002.

[23] J. D. Parsons, *The Mobile Radio Propagation Channel*, 2nd ed. John Wiley & Sons LTD, 2000.

[24] A. Alomainy, Y. Hao, X. Hu, C. Parini, and P. Hall, "UWB on-body radio propagation and system modelling for wireless body-centric networks," *IEE Proc.-Commun.*, vol. 153, no. 1, pp. 107–114, February 2006.

[25] M. Weisenhorn and W. Hirt, "ML receiver for pulsed UWB signals and parital channel state information," *IEEE International Conference on Ultra-Wideband, ICU 2005*, pp. 379–384, September 2005.

[26] S. Dubouloz, B. Denis, S. de Rivaz, and L. Ouvry, "Performance analysis of LDR UWB non-coherent receivers in multipath environments," *IEEE International Conference on Ultra-Wideband, ICU 2005*, pp. 491–496, September 2005.

Thomas Zasowski received the Dipl.-Ing. degree in electrical engineering from the Saarland University, Saarbrücken, Germany, in 2002. In 2007, he obtained the Dr. sc. ETH degree from ETH Zurich, Switzerland.

After finishing his PhD thesis in the area of UWB body area networks he stayed as postdoctoral researcher at the Communication Technology Laboratory (CTL), ETH Zurich, where he was leader of the UWB group. In 2008, he joined Swisscom Strategy & Innovation, Switzerland, where he works on future wireless communication systems.

Armin Wittneben received his M.S. and Ph.D. degrees in electrical engineering from the Technical University of Darmstadt, Germany, in 1983 and 1989 respectively.

In 1989 he joined the central research unit ASCOM Tech of ASCOM Ltd., Switzerland, as postdoctoral researcher. In 1992 he became head of the Wireless Technology and Security Department. In 1996 he also served as co-director of ASCOM Tech. In 1997 he received the Venia Legendi (Habilitation) in Communication Technology from the TU-Darmstadt. In 1998 he accepted a position as full professor of Telecommunication at the Saarland University, Germany. Since 2002 he has been full professor of Wireless Technology at ETH Zurich, Switzerland, and is serving as head of the Communication Technology Laboratory. His research interests include all aspects of wireless communication with special emphasis on communication theory, signal processing, cooperative wireless signaling and protocols, distributed MIMO systems and Ultra-Wideband/Ultra-Low Power communication.